Actinium Hydrides AcH_{10}, AcH_{12}, and AcH_{16} as High-Temperature Conventional Superconductors

Dmitrii V. Semenok,[*,†,‡] Alexander G. Kvashnin,[†,‡] Ivan A. Kruglov,[‡,§] and Artem R. Oganov[*,†,‡,§,∥]

†Skolkovo Innovation Center, Skolkovo Institute of Science and Technology, 3 Nobel Street, Moscow 143026, Russian Federation
‡Moscow Institute of Physics and Technology, 9 Institutsky Lane, Dolgoprudny 141700, Russian Federation
§Dukhov Research Institute of Automatics (VNIIA), Moscow 127055, Russian Federation
∥International Center for Materials Discovery, Northwestern Polytechnical University, Xi'an 710072, China

S *Supporting Information*

ABSTRACT: The stability of numerous unexpected actinium hydrides was predicted via the evolutionary algorithm USPEX. The electron−phonon interaction was investigated for the hydrogen-richest and most symmetric phases: $R\bar{3}m$-AcH_{10}, $I4/mmm$-AcH_{12}, and $P\bar{6}m2$-AcH_{16}. Predicted structures of actinium hydrides are consistent with all previously studied Ac−H phases and demonstrate phonon-mediated high-temperature superconductivity with T_C in the range of 204−251 K for $R\bar{3}m$-AcH_{10} at 200 GPa and 199−241 K for $P\bar{6}m2$-AcH_{16} at 150 GPa, which was estimated by directly solving the Eliashberg equation. Actinium belongs to the series of d^1 elements (Sc−Y−La−Ac) that form high-T_C superconducting (HTSC) hydrides. Combining this observation with previous predictions of p^0-HTSC hydrides (MgH_6 and CaH_6), we propose that p^0 and d^1 metals with low-lying empty orbitals tend to form phonon-mediated HTSC metal polyhydrides.
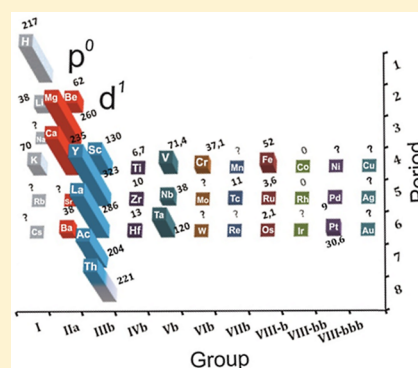
The computational search for phonon-mediated super-conductivity in binary hydrides is coming to a finale. Recent results, presented on the Mendeleev's table in Figure S1 (see the Supporting Information), show that p elements from groups IIIa−VIa form superconducting (SC) hydrides with an evenly distributed critical temperature that generally decreases with increasing period number and atomic mass of the hydride-forming atom. A completely different situation takes place for s, d, and f metals, which form a pronounced belt of superconductivity (groups IIa−IIIb, Figure S1). Recent predictions of potential high-temperature superconductivity in lanthanum and yttrium hydrides (LaH_{10} and YH_{10}[1]) and hydrides of uranium (UH_8, unpublished results), thorium (ThH_{10}, unpublished results), and scandium (ScH_6[2]) have one thing in common: all of these elements contain almost empty d, f, or p shells (MgH_6, CaH_6) and form what we call a "lability belt" (see Table 1), i.e., a zone of elements with electronic structure particularly sensitive to the atomic environment because they have empty low-lying orbitals the population of which depends on crystal field, making strong electron-phonon coupling possible.

Sequential occupation of the electronic orbitals, for example, in the lanthanide series, leads to a systematic decrease of the electron−phonon coupling (EPC) strength.[4] A possible explanation is that under high pressure electron shells with different symmetry come closer in energy and H atoms become able to form electron-deficient (e.g., 3c2e[5]) bonds with a central atom using a large number of vacant p, d, or f orbitals. Increasing the number of electrons on valence orbitals of the

Table 1. Most Promising Predicted SC Hydrides from So-Called Lability Belt

hydride	electronic configuration of the atom	calculated max T_C, K (pressure, GPa)
ScH_6	[Ar] **$3d^1$** $4s^2$	130 (200)
YH_{10}	[Kr] **$4d^1$** $5s^2$	326 (300)
LaH_{10}[a]	[Xe] **$5d^1$** $6s^2$	286 (250)
AcH_{10}	[Rn] **$6d^1$** $7s^2$	251 (this work)
ThH_{10}	[Rn] **$6d^2$** $7s^2$	221 (100)
UH_8	*[Rn] $5f^3$ **$6d^1$** $7s^2$*	*193 (0)*

[a]Structure has been confirmed experimentally.[3]

central metal atom leads to an increase of the Coulomb electron−electron repulsion that sharply reduces the electron−phonon interaction.

Another factor should also be taken into account. For heavy s^1−s^2 metals from groups I−IIa (e.g., K, Ca, Sr, Ba), the empty d shells are quite close in energy to the s shell. This means that small structural changes in the environment of the central atom may lead to large relative changes in the energy and occupation of d orbitals. This "lability factor" may help us to understand an unexpected increase of electron−phonon interaction in hydrides of boundary (s↔p, s↔d, d↔f) metals.

Verification of this hypothesis requires the study of actinide hydrides, as Ac is such a borderline element. Direct analogy of chemical properties, atomic size, electronegativity, and electronic configuration of actinium and lanthanum and recent experimental synthesis of LaH_{10+x}[3] along with predictions of near-room-temperature superconductivity in LaH_{10} at ultrahigh pressures inspired us to study the phase diagram and possible superconductivity in the Ac−H system.

Actinium (from the Greek $\alpha\kappa\tau\iota\varsigma$ − shining) is highly radioactive; its longest-lived isotope ^{227}Ac has a half-life of 22 years and in the bulk phase has a fcc crystal structure. Actinium is chemically active and its properties (valence is 3, atomic radius is 1.88 Å) are similar to lanthanum. Isotope ^{227}Ac is usually obtained by irradiation of radium with neutrons (or deuterons) in the reactor with a small yield of ~2.15%. Radioactive decay of ^{227}Ac predominantly proceeds as β^- decay with the formation of ^{227}Th and further ^{223}Ra through α-decay.[6] Thus, due to the radioactivity of daughter nuclides, ^{227}Ac is active as an α-emitter and has found application in Ac−Be neutron sources,[7] thermoelectric generators,[8] and nuclear medicine for experimental treatment of some forms of cancer, e.g., myeloid leukemia.[9] Recently, another exciting property of Ac, formation of polycations $AcHe_{17}^{3+}$ with helium, was predicted.[10] This is closely related to synthesis and study of polyhydrides (e.g., XH_{16}) as a particular case of polyatomic complexes and its stabilization by pressure or charge.

The superconductivity of metallic actinium under pressure was studied theoretically by Dakshinamoorthy et al.,[11] where the critical transition temperature (T_C) to the SC state was predicted to be from 5 to 12 K. It was also theoretically found that actinium hydride AcH_2 is metallic and undergoes multiple $Fm\bar{3}m \rightarrow P4_2/mmc \rightarrow Imma \rightarrow P6_3/mmm$ phase transitions at 12, 27, and 68 GPa, respectively.[12] Due to the high cost and radioactivity of actinium, its chemistry has been studied very poorly. In this Letter, we intend to partially fill this gap.

We built the composition−pressure phase diagram (see Figure 1), which shows pressure ranges of stability of all phases found at different pressures. As shown in Figure 1, our calculations correctly reproduce the stability of $Fm\bar{3}m$-AcH_3[13] and predict 12 new stable phases. Due to the fact that conditionally stable (extremely low-energy metastable) phases can be found in experiment, or even can dominate over thermodynamically stable phases (e.g., ref[14]), we extended the stability region for $R\bar{3}m$-AcH_{10} and $I4/mmm$-AcH_{12} to higher pressures, shown in Figure 1 by the yellow gradient and dotted lines.

Detailed information on crystal structures of the predicted phases is summarized in Table S2 (see the Supporting Information). Our calculations show that at zero pressure elemental Ac has a $P6_3/mmc$ (α-Ac) structure, which is lower in energy than $Fm\bar{3}m$-Ac (β-Ac) by 11 meV/atom and transforms to the $Fm\bar{3}m$ phase at 3 GPa. At 0 GPa, there are only two stable hydrides, metallic $Fm\bar{3}m$-AcH_2 and semiconducting $Fm\bar{3}m$-AcH_3 (DFT band gap is 0.95 eV). $Fm\bar{3}m$-AcH_2 has a fluorite-type structure with a fcc sublattice of actinium atoms, in which hydrogen atoms occupy all tetrahedral voids. The structure of $Fm\bar{3}m$-AcH_3 contains an extra H atom in the octahedral void and belongs to the Fe_3Al structure type. Phase transitions of actinium dihydride ($Fm\bar{3}m \rightarrow P4_2/mmc \rightarrow Imma \rightarrow P6_3/mmm$) predicted in ref[12] turned out to be metastable due to decomposition $2AcH_2 \rightarrow AcH + AcH_3$ in the pressure range of 5−65 GPa (see the Supporting Information).

$Fm\bar{3}m$-AcH_3 loses its stability at 78 GPa, when it transforms to $Cmcm$-AcH_3, which remains stable at least up to 350 GPa (see Figure 1). In this phase, Ac atoms are coordinated by 14 hydrogens (see the Supporting Information). Apart from AcH_2 and AcH_3, at low pressures (>5 GPa), there is another phase $Fm\bar{3}m$-AcH with a rocksalt crystal structure, which decomposes at 125 GPa ($2AcH \rightarrow Ac + P6/mmm$-$AcH_2$).

At 25 GPa, a new superhydride $Cmc2_1$-AcH_7 appears and remains stable up to 100 GPa. In this structure, Ac atoms are surrounded by 10 hydrogen atoms ($d_{Ac-H} = 2.15$−2.18 Å at 100 GPa); 4 of them are terminal atoms in stretched H_2 molecules ($d_{H-H} = 0.84$ Å compared with $d_{H-H} = 0.74$ Å in the isolated H_2 molecule), while the other 6 atoms are single hydrogens. At 50 GPa, $C2/m$-AcH_5 becomes stable (see Figure 1 and Figure S2), where Ac atoms are connected with six H atoms ($d_{Ac-H} = 2.22$ Å at 70 GPa) and two stretched H_2 molecules ($d_{H-H} = 0.85$ Å at 70 GPa). At 100 GPa, this structure undergoes a phase transition to $P\bar{1}$-AcH_5, which loses stability at 180 GPa (see Figures 1 and 2).

At 75 GPa, two new phases, $Cmmm$-Ac_3H_{10} and $Cmcm$-AcH_4, become stable (see Figure 1). $Cmcm$-AcH_4 is stable in a narrow pressure range of 75−100 GPa, whereas $Cmmm$-Ac_3H_{10}, structurally similar to $Immm$-Th_3H_{10} and $Immm$-U_3H_{10}
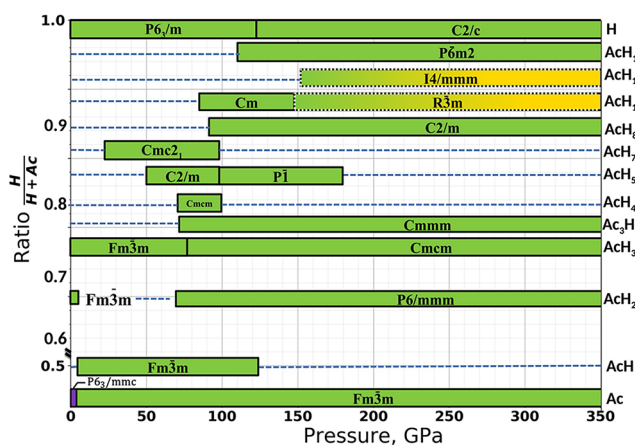
Figure 1. Pressure−composition phase diagram of the Ac−H system. Dotted lines with yellow gradient show pressure ranges where $R\bar{3}m$-AcH_{10} and $I4/mmm$-AcH_{12} may be metastable.
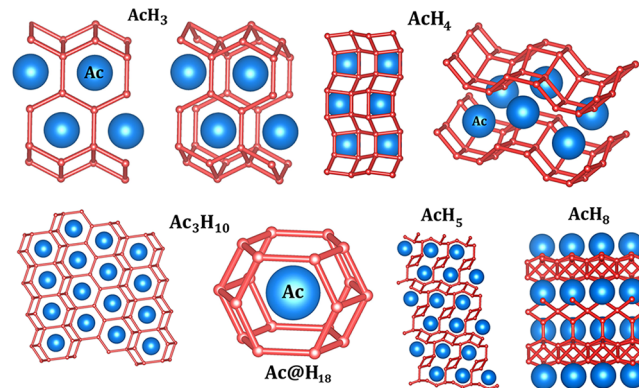

Figure 2. Crystal structures of predicted $Cmcm$-AcH_3 (150 GPa, min $d_{H-H} = 1.53$ Å), $Cmcm$-AcH_4 (100 GPa, min $d_{H-H} = 1.31$ Å in H_2 fragments), $Cmcm$-Ac_3H_{10} (150 GPa, min $d_{H-H} = 1.58$ Å), $P\bar{1}$-AcH_5 (150 GPa, min $d_{H-H} = 0.99$ Å in H_2 fragments), and $C2/m$-AcH_8 (150 GPa, min $d_{H-H} = 1.06$ Å in H_3 fragments) phases.

(unpublished results), turns out to be stable at least up to 350 GPa (Figure 1). A structurally similar phase, $Cmcm$-AcH$_3$, differs by a small displacement of hydrogen atoms (Figure 2), which indicates the possibility of easy and reversible transformation of AcH$_3$ to Ac$_3$H$_{10}$ via direct hydrogen saturation under pressure.

New metallic hydride $C2/m$-AcH$_8$ becomes stable at 90 GPa, and its structure contains bent H$_3$ groups (d_{H-H} = 1.06 Å, φ = 122° at 150 GPa), and each Ac atom is bonded to three H$_3$ fragments (Supporting Information, Figure S2).

At 80 GPa, actinium decahydride (Cm-AcH$_{10}$) appears on the phase diagram. At around 140 GPa, it transforms to a more symmetric $R\overline{3}m$-AcH$_{10}$. The stability of $R\overline{3}m$-AcH$_{10}$ is determined by the enthalpy of reaction: AcH$_{10}$ → 3AcH$_8$ + AcH$_{16}$, which is ΔH = 0.175 eV at 150 GPa (0 K) and ΔH = −1.628 eV at 250 GPa (0 K) when taking into account the zero-point energy (ZPE) contribution. Taking vibrational contribution to the free energy into account, we find that the stability field of $R\overline{3}m$-AcH$_{10}$ expands at room or higher temperatures.

In $R\overline{3}m$-AcH$_{10}$ (150 GPa), the first coordination sphere of Ac contains 14 hydrogen atoms at d_{Ac-H} = 2.10 Å (see Figure 3a).
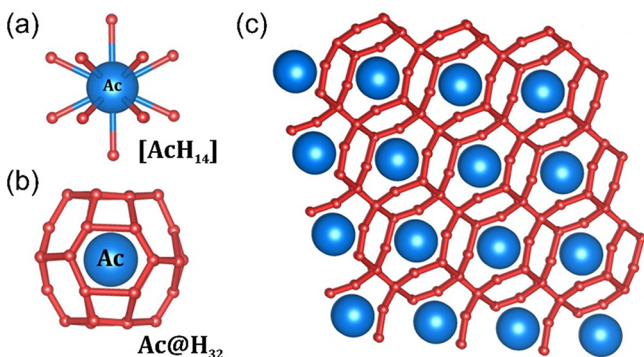
Figure 3. Structural features of $R\overline{3}m$-AcH$_{10}$ at 150 GPa. (a) First coordination sphere of Ac atom containing 14 hydrogens; (b) hydrogen polyhedral cage around each Ac atom; (c) crystal structure of AcH$_{10}$.

The hydrogen environment of Ac atoms can also be described as clathrate-like cage with 32 hydrogen atoms with a diameter of ∼4.5 Å (see Figure 3b). The shortest H−H distance is 1.07 Å.

The metastable $I4/mmm$-AcH$_{12}$ was studied in the pressure range of 150−300 GPa. The existence of this compound is determined by two possible reactions: 3AcH$_{12}$ → 2AcH$_{10}$ +

AcH$_{16}$ and 2AcH$_{12}$ → AcH$_8$ + AcH$_{16}$. Calculations indicate that ZPE and thermal contributions play a minor role here, and AcH$_{12}$ remains metastable (above the convex hull by 0.05−0.06 eV/atom).

The hydrogen environment of Ac atoms in $I4/mmm$-AcH$_{12}$ can be described as clathrate-like cage with 40 hydrogen atoms with a diameter of ∼4.47 Å (see Figure 4a). The coordination sphere of Ac in $I4/mmm$-AcH$_{12}$ is made of eight H atoms (see Figure 4b) at d_{Ac-H} = 2.06 Å and another eight H atoms at d_{Ac-H} = 2.11 Å at 150 GPa. The connection between [AcH$_{16}$] (Figure 4b) is carried out via H$_4$ tetrahedra with d_{H-H} = 1.45 Å, but the minimum H−H distance in AcH$_{12}$ is in almost linear (φ = 170°) H$_3$ fragments with d_{H-H} = 0.94 Å (see Figure 4b,c).

An interesting metallic $P\overline{6}m2$-AcH$_{16}$ phase is found to be stable at 110 GPa, in which Ac atoms are coordinated by 12 hydrogens with d_{Ac-H} = 2.08 Å at 150 GPa (see Figure 5a). Extension of the radius of the coordination sphere up to 2.16 Å leads to addition of 12 more H atoms to the coordination sphere (Figure 5b). These 12 H atoms form 6 H$_2$ molecules (d_{H-H} = 0.87 Å). Thus, in [Ac(hex-H$_6$)$_2$](H$_2$)$_6$, Ac atoms along with 24 bounded H atoms form the hexagonal lattice shown in Figure 5d.

Among all predicted hydrogen-rich phases, only two are semiconducting ($C2/m$-AcH$_5$ and $Cmc2_1$-AcH$_7$) with DFT band gaps of 0.56 and 1.58 eV, respectively; the systematic underestimation of the band gap by the DFT-PBE method should be kept in mind (see the Supporting Information for details). The rest of the predicted phases are metallic and are potential high-temperature superconductors. Phonon calculations confirmed that the predicted phases have no imaginary phonon frequencies in their predicted ranges of thermodynamic stability (see the Supporting Information). The most interesting compounds AcH$_{10}$, AcH$_{12}$, and AcH$_{16}$ were confirmed to be non-magnetic.

T_C was calculated using the "full" Allen−Dynes formula (see eq 1) and the Allen−Dynes modified McMillan formula; see Table 2. We calculated the Eliashberg function $\alpha^2F(\omega)$ at different pressures (see the Supporting Information). One can note that an increase of pressure leads to shifting of the $\alpha^2F(\omega)$ function to higher frequencies. Our calculations indicate that $\alpha^2F(\omega)$ Eliashberg functions of $R\overline{3}m$-AcH$_{10}$ at 200 GPa (see Figure 6a) and $P\overline{6}m2$-AcH$_{16}$ at 150 GPa (see the Supporting Information) have one main "hill". For this type of $\alpha^2F(\omega)$ function, the numerical solution of the Eliashberg equations is well approximated by the full Allen−Dynes formula.[15] Calculated λ and ω_{log} as a function of pressure for $R\overline{3}m$-
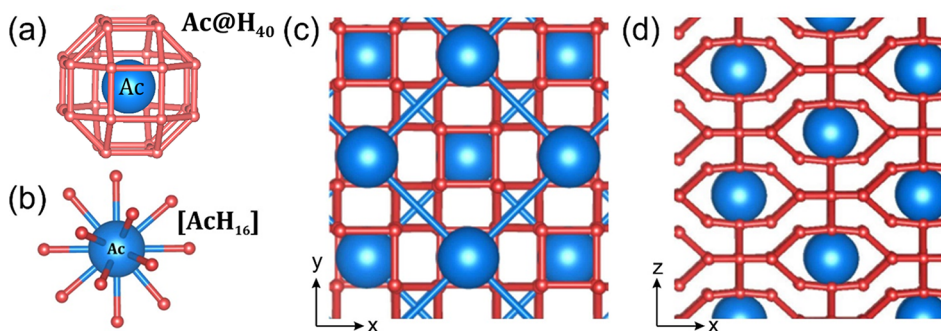
Figure 4. Structural features of $I4/mmm$-AcH$_{12}$ at 150 GPa. (a) Coordination sphere of the Ac atom containing 16 hydrogen atoms; (b) top and (c) side views of $I4/mmm$-AcH$_{12}$.
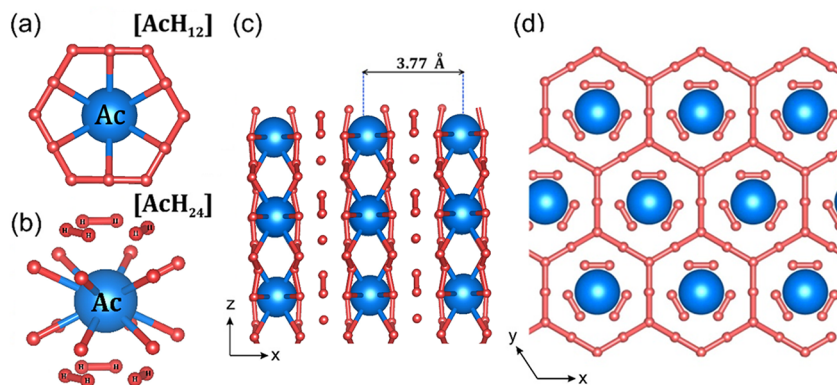
Figure 5. Structural features of $P\bar{6}m2$-AcH_{16} at 150 GPa. (a) First coordination sphere of Ac atom with 12 hydrogen atoms; (b) coordination of Ac atom by 24 hydrogen atoms; (c) side view of $P\bar{6}m2$-AcH_{16}; (d) top view of $P\bar{6}m2$-AcH_{16}.

Table 2. Predicted SC Properties of Actinium Hydrides[a]

phase	P, GPa	λ	N_{f_i}, states/atom/eV	ω_{log}, K	T_C (McMillan), K	T_C (Allen–Dynes), K	T_C (Eliashberg), K
$Cmcm$-AcH_3	150	0.05	0.094	486	0	0	0
$Cmmm$-Ac_3H_{10}	150	0.39	0.071	803.6	3 (0.55)	3 (0.55)	3 (0.55)
$Cmcm$-AcH_4	100	0.89	0.071	982.5	56.5 (41.2)	60 (43.2)	67 (50)
$P\bar{1}$-AcH_5	150	0.92	0.071	1162	70.5 (49.8)	74.9 (52)	79 (61)
$C2/m$-AcH_8	150	1.79	0.052	853	113.5 (99.5)	134 (114.1)	149 (134)
Cm-AcH_{10}	100	2.18	0.057	791.3	120.4 (107.9)	152.1 (130.5)	177 (162)
$R\bar{3}m$-AcH_{10}	200	3.46	0.068	710.9	160.9 (125.5)	204.1 (177)	251 (226)
	250	1.96	0.072	812.8	115.3 (102.2)	140.1 (119.7)	176 (151)
	300	1.01	0.074	1098	77.3 (59.7)	83.2 (63.3)	101 (76)
$I4/mmm$-AcH_{12}	150	1.97	0.044	697	99.4 (87.3)	123.3 (103.7)	173 (148)
	300	1.42	0.041	677	73.4 (62)	83.8 (68.9)	101 (81)
$P\bar{6}m2$-AcH_{16}	150	2.16	0.022	1054	159.7 (143)	199.2 (171.3)	241 (221)
	250	1.34	0.046	1383	140.5 (118.2)	155.9 (128.5)	181 (163)

[a]T_C values are given for μ^* equal to 0.1, while T_C values in brackets are for $\mu^* = 0.15$.
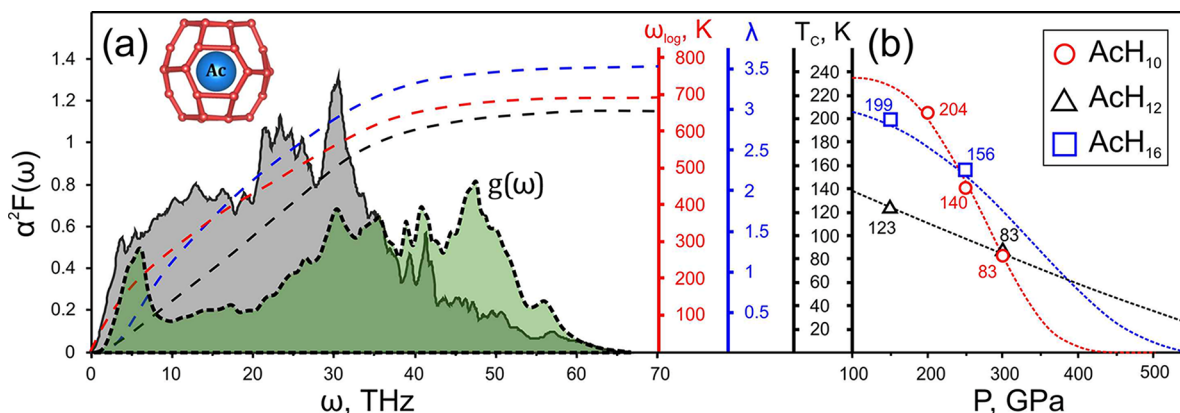
Figure 6. (a) Eliashberg function $\alpha^2F(\omega)$, ω_{log}, EPC coefficient λ, critical transition temperature (T_C), and phonon DOS (au) of $R\bar{3}m$-AcH_{10} at 200 GPa; (b) $T_C(P)$ functions for $R\bar{3}m$-AcH_{10}, $I4/mmm$-AcH_{12}, and $P\bar{6}m2$-AcH_{16}.

AcH_{10}, $I4/mmm$-AcH_{12}, and $P\bar{6}m2$-AcH_{16} are summarized in Table 2.

As we mentioned above, the following new stable or conditionally stable phases are metallic and potentially high-T_C superconductors: $Cmcm$-AcH_3, $Cmcm$-AcH_4, $Cmcm$-Ac_3H_{10}, $P\bar{1}$-AcH_5, $C2/m$-AcH_8, $R\bar{3}m$-AcH_{10}, $I4/mmm$-AcH_{12}, and $P\bar{6}m2$-AcH_{16}. For AcH_8, AcH_{10}, AcH_{12}, and AcH_{16}, the EPC coefficient λ exceeds 1.5, and the "full" eq 1 was used for calculating T_C.

$Cmcm$-AcH_3 is not a superconductor due to the very low EPC coefficient of <0.1 leading to T_C close to 0 K. Calculations

of T_C for $Cmcm$-Ac_3H_{10} and $Cmcm$-AcH_4 phases give 3 K ($\lambda = 0.39$) and 60 K ($\lambda = 0.89$), respectively. This can be explained by the increasing symmetry and hydrogen content versus $Cmcm$-AcH_3. However, an increase in hydrogen content leads to new phenomena in AcH_5: there are two stable phases, semiconducting $C2/m$-AcH_5 (stable below 100 GPa) and low-symmetry metallic $P\bar{1}$-AcH_5 (above 100 GPa), with relatively high SC parameters ($\lambda = 0.92$, $\omega_{log} = 1162$ K). This behavior can be explained by structural differences; in $C2/m$-AcH_5, the hydrogen sublattice consists of H_2 and isolated H atoms that together forms isolated distorted hexagons, while in $P\bar{1}$-AcH_5,

the hydrogen sublattice consists of bent H_3 groups that form infinite hydrogen chains.

The same explanation may be applied for $Cmc2_1$-AcH_7 (semiconductor, stable at <100 GPa), consisting of isolated H_2 and H_4 groups, and $C2/m$-AcH_8 (metal, stable at >100 GPa) with unexpectedly high SC parameters ($\lambda = 1.79$, $T_C = 114-134$ K; see Table 2). AcH_8 contains bent H_3 groups that form a well-connected branched three-dimensional net.

The highest transition temperature was calculated for $R\bar{3}m$-AcH_{10} to be in a range from 177 to 204 K at 200 GPa (according to the Allen–Dynes equation), depending on the exact μ^* value (see Table 2 and Figure 6a). Comparison of $\alpha^2F(\omega)$ with the phonon density of states (DOS) (light green) shows that low-frequency modes of the H_{32} cage provide the main contribution to SC. The effect of high-frequency oscillations of H_2 fragments is very weak. Thus, for a certain hydrogen content (Ac/H = 1:10), specific for each element, the maximum parameters of the electron–phonon interaction are reached. Further increase of hydrogen content in actinium hydrides ($I4/mmm$-AcH_{12}) does not lead to higher T_C. Only $P\bar{6}m2$-AcH_{16} below 150 GPa can achieve 200 K (see Figure 6b). As can be seen from Table 2, in the series of hydrides AcH_{3-10}, the critical temperature increases monotonically as the concentration of hydrogen atoms increases, but further increase of hydrogen concentration leads to decrease of T_C decreasing.

For the hydrogen-richest phases, $R\bar{3}m$-AcH_{10}, $I4/mmm$-AcH_{12}, and $P\bar{6}m2$-AcH_{16}, the dependence of EPC parameters on pressure was studied and extrapolated via the well-known empirical equation for low-T_C superconductors,[30,31]

$$-\ln\left(\frac{T_C}{\omega_{\log}}\right) = Cv^{-\varphi}, \quad C > 0,$$ where v is the volume and C and φ parameters were calculated earlier for nontransition metals ($\varphi = 2.5 \pm 0.6$).[16,17] The computed decrease of T_C with pressure for AcH_{10}, $dT_C/dP = -1.21$ K/GPa (at 250 GPa), is much steeper than that for AcH_{12}, $dT_C/dP = -0.263$ K/GPa (at 250 GPa), and that for AcH_{16}, $dT_C/dP = -0.433$ K/GPa at 250 GPa (see Figure 6b). For comparison, for CaH_6, $dT_C/dP = -0.33$ K/GPa.[18] From calculated data (interpolation of the $\ln[T_C/\omega_{\log}]$ function by the $a \times v^b$ law), we can directly determine the coefficients $\varphi = 5.53$ (AcH_{10}), 0.89 (AcH_{12}), and 1.76 (AcH_{16}), which are far from the values for low-temperature superconductors. Obtained extrapolation of $T_C(P)$ is shown in Figure 6b. $I4/mmm$-AcH_{12} was found to be the least sensitive to pressure change. The layer-like character of $P\bar{6}m2$-AcH_{16} leads to substantially higher response to pressure changes in the DOS (increases 2 times in the pressure range of 150–250 GPa) as well as in EPC parameters (see Table 2).

Following the analogy between lanthanum and actinium, in the expected manner, $R\bar{3}m$-AcH_{10} possesses remarkable high-temperature superconductivity ($T_C = 226-251$ K) and structural similarity to the recently synthesized LaH_{10+x}.[3] Besides AcH_{10}, we found two more SC hydrides: $I4/mmm$-AcH_{12} and $P\bar{6}m2$-AcH_{16}. Similarity of structures of LaH_{10} and AcH_{10} suggests that La may also have hydrides similar to AcH_{12} and AcH_{16}, and these (LaH_{12}, LaH_{16}) compounds as well as La_3H_{10} may have been missed by a previous search.[1]

In conclusion, exploring the analogy between the electronic structure of actinium and lanthanum atoms, we hypothesized that the Ac–H system may have high-T_C SC phases and studied Ac–H system using global optimization within the evolutionary algorithm USPEX at pressures up to 350 GPa.

Five new high-temperature superconductors were predicted, namely $C2/m$-AcH_8, Cm- and $R\bar{3}m$-AcH_{10}, $I4/mmm$-AcH_{12} and $P\bar{6}m2$-AcH_{16}. AcH_{10} is predicted to be SC at temperatures up to 251 K at 200 GPa, AcH_{16} − at temperatures up to 241 K at 110 GPa.

This study is an important part of the work on establishing chemical insight into SC properties of binary metal hydrides, which has a clear correlation with the electronic structure of the hydride-forming metal. Namely, we found that the majority of high-T_C SC hydrides are concentrated near the d^1f^0 belt of the Periodic Table that is, among metals with minimal number of d and f electrons. With an increasing number of d and f-electrons, SC properties of metal hydrides become less pronounced, possibly due to increasing Coulomb electron–electron repulsion. Large groups of high-temperature hydride superconductors are tied to specific generative metals lying on the junctions (p–d, s–p) of p, d, and f groups of elements.

This work contributes to the establishment of extreme diversity of actinide hydrides, which, as we have shown earlier (unpublished results), are unexpectedly rich in high-temperature SC phases.

Methods. Evolutionary algorithm USPEX[19−21] is a powerful tool for prediction of thermodynamically stable compounds of given elements at a given pressure (for some of its application, see refs 22−24). We performed variable-composition searches in the Ac−H system at pressures of 0, 50, 150, 250, and 350 GPa. The first generation (110 structures) was created using a random symmetric generator, while all subsequent generations contained 20% random structures and 80% were created using heredity, softmutation, and transmutation operators.

Here, evolutionary investigations were combined with structure relaxations and total energy calculations using density functional theory (DFT)[25,26] within the generalized gradient approximation (Perdew−Burke−Ernzerhof functional)[27] and the projector augmented wave method,[28,29] as implemented in the VASP code.[30−32] The plane-wave kinetic energy cutoff was set to 600 eV, and the Brillouin zone was sampled by Γ-centered k-point meshes with resolution $2\pi \times 0.05$ Å^{-1}.

In order to establish stability fields of the predicted phases, we recalculated their enthalpies with increased precision at various pressures with a smaller pressure increment (from 5 to 10 GPa), recalculating the thermodynamic convex hull (Maxwell construction) at each pressure. By definition, the thermodynamically stable phase has lower Gibbs free energy (or, at zero Kelvin, lower enthalpy) than any phase or phase assembly of the same composition. Phases that were located on the convex hull are the ones stable at a given pressure. Stable structures of elemental Ac, H, and AcH_3 were taken from USPEX calculations and agree with those from refs 13 and 33.

Calculations of SC T_C were carried out using the QUANTUM ESPRESSO package.[34] Phonon frequencies and EPC coefficients were computed using density functional perturbation theory,[35] employing the plane-wave pseudopotential method and Perdew−Burke−Ernzerhof exchange−correlation functional.[27] The effects of core electrons of Ac on valence wave functions were modeled with the aid of scalar relativistic ultrasoft pseudopotentials.[36] The $6s^2p^6d^17s^2$ electrons of Ac were treated explicitly. Convergence tests showed that 80 Ry is a suitable kinetic energy cutoff for the plane-wave basis set.

Electronic band structures of newly found actinium hydrides were calculated using both VASP and QE and demonstrated good consistency. Comparison of phonon densities of states calculated using a finite displacement method (VASP and

PHONOPY[37,38]) and density functional perturbation theory (QE) showed perfect agreement between these methods.

The critical temperature was calculated from the Eliashberg equation,[39] which is based on the Fröhlich Hamiltonian $\hat{H} = \hat{H}_e + \hat{H}_{ph} + \sum_{k,q,j} g^{q,j}_{k+q,k} \hat{c}^+_{k+q} \hat{c}_k (\hat{b}^+_{-q,j} + \hat{b}_{q,j})$, where c^+ and b^+ relate to creation operators of electrons and phonons, respectively. The matrix element of electron−phonon interaction $g^{q,j}_{k+q,k}$ calculated within the harmonic approximation in Quantum E S P R E S S O c a n b e d e f i n e d a s $g_{k+\frac{q}{q},k}^{j} = \sqrt{\frac{\hbar}{2M\omega_{q,j}}} \int \psi_k^*(r) \cdot \left\{ \frac{dV_{scf}}{d\vec{u_q}} \cdot \frac{\vec{u_q}}{|\vec{u_q}|} \right\} \cdot \psi_{k+q}(r)\, d^3 r$, where u_q is the displacement of an atom with mass M in the phonon mode q,j. Within the framework of the Gor'kov and Migdal approach,[40,41] the correction to the electron Green's function $\sum(\vec{k}, \omega) = G_0^{-1}(\vec{k}, \omega) - G^{-1}(\vec{k}, \omega)$ caused by interaction can be calculated by taking into account only the first terms of the expansion of electron−phonon interaction in series of (ω_{log}/E_F). As a result, it will lead to integral Eliashberg equations.[39] These equations can be solved by an iterative self-consistent method for the real part of the order parameter $\Delta(T, \omega)$ (SC gap) and the mass renormalization function $Z(T, \omega)$[42] (see the Supporting Information).

In our ab initio calculations of the EPC parameter λ, the first Brillouin zone was sampled using a $4 \times 4 \times 4$ q-point mesh and a denser $24 \times 24 \times 24$ k-point mesh (with Gaussian smearing and $\sigma = 0.02$ Ry, which approximates the zero-width limits in the calculation of λ). The SC transition temperature T_C was also estimated by using two equations: "full" Allen−Dynes and "short" modified McMillan equation.[15] The full Allen−Dynes equation for calculating T_C has the following form[15]

$$T_C = \omega_{log} \frac{f_1 f_2}{1.2} \exp\left(\frac{-1.04(1 + \lambda)}{\lambda - \mu^* - 0.62\lambda\mu^*} \right) \quad (1)$$

with

$$f_1 f_2 = \sqrt[3]{1 + \left(\frac{\lambda}{2.46(1 + 3.8\mu^*)} \right)^{3/2}} \cdot \left(1 - \frac{\lambda^2(1 - \omega_2/\omega_{log})}{\lambda^2 + 3.312(1 + 6.3\mu^*)^2} \right) \quad (2)$$

while the modified McMillan equation has the form but with $f_{1*}f_2 = 1$.

The EPC constant λ, logarithmic average frequency ω_{log}, and mean-square frequency ω_2 were calculated as

$$\lambda = \int_0^{\omega_{max}} \frac{2 \cdot \alpha^2 F(\omega)}{\omega}\, d\omega \quad (3)$$

and

$$\omega_{log} = \exp\left(\frac{2}{\lambda} \int_0^{\omega_{max}} \frac{d\omega}{\omega} \alpha^2 F(\omega) \ln(\omega) \right)$$

$$\omega_2 = \sqrt{\frac{1}{\lambda} \int_0^{\omega_{max}} \left[\frac{2\alpha^2 F(\omega)}{\omega} \right] \omega^2\, d\omega} \quad (4)$$

where μ^* is the Coulomb pseudopotential, for which we used widely accepted lower and upper bounds of 0.10 and 0.15.

ASSOCIATED CONTENT

Ⓢ Supporting Information

The Supporting Information is available free of charge on the ACS Publications website at DOI: 10.1021/acs.jpclett.8b00615.

Crystal data of predicted Ac−H phases, detailed information about the thermodynamical stability of studied phasesm and calculated densities of electronic and phonon states along with Eliashberg functions (PDF)

AUTHOR INFORMATION

Corresponding Authors
*E-mail: dmitrii.semenok@skolkovotech.ru (D.V.S.).
*E-mail: A.Oganov@skoltech.ru (A.R.O.).

ORCID ⓘ
Dmitrii V. Semenok: 0000-0002-1374-9091
Alexander G. Kvashnin: 0000-0002-0718-6691

Notes
The authors declare no competing financial interest.

REFERENCES

(1) Liu, H.; Naumov, I. I.; Hoffmann, R.; Ashcroft, N. W.; Hemley, R. J. Potential High-Tc Superconducting Lanthanum and Yttrium Hydrides at High Pressure. *Proc. Natl. Acad. Sci. U. S. A.* **2017**, *114*, 6990−6995.

(2) Qian, S.; Sheng, X.; Yan, X.; Chen, Y.; Song, B. Theoretical Study of Stability and Superconductivity of ScHn (N = 4−8) at High Pressure. *Phys. Rev. B: Condens. Matter Mater. Phys.* **2017**, *96*, 094513−094519.

(3) Geballe, Z. M.; Liu, H.; Mishra, A. K.; Ahart, M.; Somayazulu, M.; Meng, Y.; Baldini, M.; Hemley, R. J. Synthesis and Stability of Lanthanum Superhydrides. *Angew. Chem., Int. Ed.* **2018**, *57* (3), 688−692.

(4) Peng, F.; Sun, Y.; Pickard, C. J.; Needs, R. J.; Wu, Q.; Ma, Y. Hydrogen Clathrate Structures in Rare Earth Hydrides at High Pressures: Possible Route to Room-Temperature Superconductivity. *Phys. Rev. Lett.* **2017**, *119*, 107001−107007.

(5) Struzhkin, V. V.; Kim, D. Y.; Stavrou, E.; Muramatsu, T.; Mao, H.; Pickard, C. J.; Needs, R. J.; Prakapenka, V. B.; Goncharov, A. F. Synthesis of Sodium Polyhydrides at High Pressures. *Nat. Commun.* **2016**, *7*, 12267.

(6) Audi, G.; Bersillon, O.; Blachot, J.; Wapstra, A. H. The Nubase Evaluation of Nuclear and Decay Properties. *Nucl. Phys. A* **2003**, *729* (1), 3−128.

(7) Alaerts, L.; Op De Beeck, J. P.; Hoste, J. An227Ac-Be Isotopic Neutron Source for Application in High-Accuracy Neutron Activation Analysis. *Anal. Chim. Acta* **1974**, *69* (1), 1−9.

(8) Gammel, G.; Koskinen, M. F.; De Toyer, A. *Raumfahrtforschung. Band XIII*; Deutschen Gesellschaft für Raketentechnik und Raumfahrt e. V., 1969.

(9) Scheinberg, D. A.; McDevit, M. R. Actinium-225 in Targeted Alpha-Particle Therapeutic Applications. *Curr. Radiopharm.* **2011**, *4* (4), 306−320.

(10) Kaltsoyannis, N. Seventeen-Coordinate Actinide Helium Complexes. *Angew. Chem., Int. Ed.* **2017**, *56* (25), 7066−7069.

(11) Dakshinamoorthy, M.; Iyakutti, K. Band Structure, Fermi Surface, Superconductivity, and Resistivity of Actinium under High Pressure. *Phys. Rev. B: Condens. Matter Mater. Phys.* **1984**, *30* (12), 6943−6950.

(12) Jiang, H.; Wang, W.; Zhang, C.; Hu, X.-N.; Zhong, G.-H.; Lu, X.-Q.; Su, Y.-H. Phase Transitions of Actinium Dihydride: Pressure-Induced Charge Transfer Driving Effect. *Int. J. Hydrogen Energy* **2014**, *39* (28), 15827−15835.

(13) Farr, J. D.; Giorgi, A. L.; Bowman, M. G.; Money, R. K. The Crystal Structure of Actinium Metal and Actinium Hydride. *J. Inorg. Nucl. Chem.* **1961**, *18*, 42−47.

(14) Flores-Livas, J. A.; Sanna, A.; Drozdov, A. P.; Boeri, L.; Profeta, G.; Eremets, M.; Goedecker, S. Interplay between Structure and Superconductivity: Metastable Phases of Phosphorus under Pressure. *Phys. Rev. Mater.* **2017**, *1*, 024802−024810.

(15) Allen, P. B.; Dynes, R. C. Transition Temperature of Strong-Coupled Superconductors Reanalyzed. *Phys. Rev. B* **1975**, *12* (3), 905−922.

(16) Rohrer, H. Druck- und Volumeneffekte in der Supraleitung. *Helv. Phys. Acta* **1960**, *33*, 675−705.

(17) Olsen, J. L.; Rohrer, H. The volume dependence of the electron level density and the critical temperature in superconductors. *Helv. Phys. Acta* **1960**, *33*, 872−880.

(18) Wang, H.; Tse, J. S.; Tanaka, K.; Iitaka, T.; Ma, Y. Superconductive Sodalite-like Clathrate Calcium Hydride at High Pressures. *Proc. Natl. Acad. Sci. U. S. A.* **2012**, *109* (17), 6463−6466.

(19) Oganov, A. R.; Glass, C. W. Crystal Structure Prediction Using Ab Initio Evolutionary Techniques: Principles and Applications. *J. Chem. Phys.* **2006**, *124*, 244704.

(20) Oganov, A. R.; Lyakhov, A. O.; Valle, M. How Evolutionary Crystal Structure Prediction Works—and Why. *Acc. Chem. Res.* **2011**, *44*, 227−237.

(21) Lyakhov, A. O.; Oganov, A. R.; Stokes, H. T.; Zhu, Q. New Developments in Evolutionary Structure Prediction Algorithm USPEX. *Comput. Phys. Commun.* **2013**, *184*, 1172−1182.

(22) Ma, Y.; Eremets, M.; Oganov, A. R.; Xie, Y.; Trojan, I.; Medvedev, S.; Lyakhov, A. O.; Valle, M.; Prakapenka, V. Transparent Dense Sodium. *Nature* **2009**, *458* (7235), 182−185.

(23) Duan, D.; Liu, Y.; Tian, F.; Li, D.; Huang, X.; Zhao, Z.; Yu, H.; Liu, B.; Tian, W.; Cui, T. Pressure-Induced Metallization of Dense (H2S)2H2 with High-Tc Superconductivity. *Sci. Rep.* **2015**, *4*, 6968.

(24) Dong, X.; Oganov, A. R.; Goncharov, A. F.; Stavrou, E.; Lobanov, S.; Saleh, G.; Qian, G.-R.; Zhu, Q.; Gatti, C.; Deringer, V. L.; et al. A Stable Compound of Helium and Sodium at High Pressure. *Nat. Chem.* **2017**, *9* (5), 440−445.

(25) Hohenberg, P.; Kohn, W. Inhomogeneous Electron Gas. *Phys. Rev.* **1964**, *136* (3B), B864−B871.

(26) Kohn, W.; Sham, L. J. Self-Consistent Equations Including Exchange and Correlation Effects. *Phys. Rev.* **1965**, *140* (4), A1133−A1138.

(27) Perdew, J. P.; Burke, K.; Ernzerhof, M. Generalized Gradient Approximation Made Simple. *Phys. Rev. Lett.* **1996**, *77* (18), 3865−3868.

(28) Blöchl, P. E. Projector Augmented-Wave Method. *Phys. Rev. B: Condens. Matter Mater. Phys.* **1994**, *50* (24), 17953−17979.

(29) Kresse, G.; Joubert, D. From Ultrasoft Pseudopotentials to the Projector Augmented-Wave Method. *Phys. Rev. B: Condens. Matter Mater. Phys.* **1999**, *59* (3), 1758−1775.

(30) Kresse, G.; Furthmüller, J. Efficient Iterative Schemes for Ab Initio Total-Energy Calculations Using a Plane-Wave Basis Set. *Phys. Rev. B: Condens. Matter Mater. Phys.* **1996**, *54*, 11169−11186.

(31) Kresse, G.; Hafner, J. Ab Initio Molecular Dynamics for Liquid Metals. *Phys. Rev. B: Condens. Matter Mater. Phys.* **1993**, *47*, 558−561.

(32) Kresse, G.; Hafner, J. Ab Initio Molecular-Dynamics Simulation of the Liquid-Metal Amorphous-Semiconductor Transition in Germanium. *Phys. Rev. B: Condens. Matter Mater. Phys.* **1994**, *49*, 14251−14269.

(33) Pickard, C. J.; Needs, R. J. Structure of Phase III of Solid Hydrogen. *Nat. Phys.* **2007**, *3* (7), 473−476.

(34) Giannozzi, P.; Baroni, S.; Bonini, N.; Calandra, M.; Car, R.; Cavazzoni, C.; Ceresoli, D.; Chiarotti, G. L.; Cococcioni, M.; Dabo, I.; et al. QUANTUM ESPRESSO: A Modular and Open-Source Software Project for Quantum Simulations of Materials. *J. Phys.: Condens. Matter* **2009**, *21*, 395502.

(35) Baroni, S.; de Gironcoli, S.; Dal Corso, A.; Giannozzi, P. Phonons and Related Crystal Properties from Density-Functional Perturbation Theory. *Rev. Mod. Phys.* **2001**, *73* (2), 515−562.

(36) Vanderbilt, D. Soft Self-Consistent Pseudopotentials in a Generalized Eigenvalue Formalism. *Phys. Rev. B: Condens. Matter Mater. Phys.* **1990**, *41* (11), 7892.

(37) Togo, A.; Tanaka, I. First Principles Phonon Calculations in Materials Science. *Scr. Mater.* **2015**, *108*, 1−5.

(38) Togo, A.; Oba, F.; Tanaka, I. First-Principles Calculations of the Ferroelastic Transition between Rutile-Type and CaCl2-Type SiO2 at High Pressures. *Phys. Rev. B: Condens. Matter Mater. Phys.* **2008**, *78*, 134106.

(39) Eliashberg, G. M. Interactions between Electrons and Lattice Vibrations in a Superconductor. *JETP* **1959**, *11* (3), 696−702.

(40) Gor'kov, L. P. On Energy Spectrum of Superconductors. *JETP* **1958**, *34*, 735.

(41) Migdal, A. B. Interaction between Electrons and Lattice Vibrations in a Normal Metal. *JETP* **1958**, *34* (7), 996−1001.

(42) Maksimov, E. G.; Savrasov, D. Y.; Savrasov, S. Y. The Electron-Phonon Interaction and the Physical Properties of Metals. *Phys.-Usp.* **1997**, *40* (4), 337.